External stress as a way to control Au(111) reconstruction

D. Chauraud, J. Durinck, L. Vernisse, S. Smalley, M. Drouet, C. Coupeau

Version of Record: https://www.sciencedirect.com/science/article/pii/S0039602821001126
Manuscript_a68666ca01cf2e76fc8262c13f9f66ed

External stress as a way to control Au(111) reconstruction

D. Chauraud[a], J. Durinck[b,*], L. Vernisse[b], S. Smalley[b], M. Drouet[b], C. Coupeau[b]

[a]*Department of Materials Science and Engineering, Institute I, Friedrich-Alexander-Universität Erlangen-Nürnberg (FAU), Germany*
[b]*Institut P', UPR 3346 CNRS, Université de Poitiers-ENSMA-CNRS, France*

Abstract

We report investigations on gold single crystals carried out with the help of an original experimental set-up, combining a scanning tunneling microscope and a compression device under ultra high vacuum, that allows for *in situ* observations of stressed surfaces at the atomic scale. It is observed that a macroscopic compression strain may induce a reorganization of the Au(111) surface reconstruction, known as the chevron-like pattern. Molecular dynamics simulations using a modified embedded atom method potential have been carried out to highlight the elementary dislocation mechanisms at the origin of such an evolution.

Keywords: Surface Reconstruction, Scanning Tunneling Microscopy, Molecular Dynamics

Many techniques have been developed to achieve periodic patterns at different scales ranging from approximately ten micrometers to ten nanometers. These include lithographic techniques, focused ion beam spraying or

*Corresponding author
Email address: julien.durinck@univ-poitiers.fr (J. Durinck)

ionic spray at grazing incidence. The ultimate step in designing new materials at nano or atomic scale is to now modulate and control atomic surfaces, such as vicinal steps [1, 2, 3, 4, 5] or surface reconstructions [6, 7, 8, 9, 10, 11, 12]. These surfaces may then be used as specific templates for molecule or nanoparticle depositions. From this perspective, the Au(111) surface deserves special attention due to its particular $22 \times \sqrt{3}$ reconstruction [13, 7, 6, 14], known in the literature as a herringbone or chevron-like pattern. This reconstruction has been of use in the self-organization of molecules [15, 16, 17] or metallic clusters [18, 19, 20, 21] for applications in nanoelectronics, information storage or nanocatalysis [22, 20]. It was also recently shown that single-strand deoxyribonucleic acid (DNA) deposited on the Au(111) surface could be an interesting candidate for the integration of DNA into solid nanodevices [23]. The chevron-like pattern can be influenced by the presence of vicinal steps and, in particular, it has been suggested that the chevron organization depends on the faceting of the vicinal steps, {100} or {111} [24, 25]. It has also been observed, both experimentally by scanning tunneling microscopy (STM) and numerically with atomistic simulations, that the period of the herringbone pattern increases with the decrease of the atomic terrace width [26]. More recently, Chauraud *et al.* have highlighted a re-organization of the reconstruction induced by slip traces that result from the emergence at the free surface of moving dislocations in the bulk [27]. Although the Au(111) reconstruction has been the subject of extensive studies in the past, only a few are concerned with the influence of strain/stress on the chevron organization. The most significant work on this subject has been proposed by Schaff *et al.* [28]. In this study, the authors have strained Au(111)-oriented films

on mica substrates using a bending apparatus. Their STM observations of the surface have highlighted a clear evolution of the Au(111) reconstruction under stress, from a 2D herringbone pattern to a 1D configuration. In this paper, *in situ* STM investigations of Au single crystals under controlled uniaxial applied stress have been carried out using the original set-up Nanoplast [29]. The effect of a macroscopic compression stress on the chevron pattern is first presented and then discussed in the framework of molecular dynamics simulations performed at the same atomic scale.

The dislocation network describing the Au(111) reconstruction is presented in Fig. 1. It consists of partial Shockley dislocations of type $1/6\,\langle 112\rangle$ (black bold line in Fig. 1). For convenience, the (111) face of the Thompson tetrahedron is also shown in Fig. 1. The partial dislocation Burgers vectors correspond to Xδ (or δX) with X = A, B or C. Three variants thus exist due to the three-fold symmetry of the Au(111) surface. Each pair of partial dislocations arises from the dissociation of $1/2\,\langle 110\rangle$ perfect edge dislocations. For instance, the perfect edge CA dislocation is dissociated into Cδ and δA on the left side of the schematic in Fig. 1, leading to alternating hexagonal close packed (hcp) and face centered cubic (fcc) stacking areas along the $[0\bar{1}1]$ direction. The partial dislocations are lying along the $\langle 112\rangle$ directions, parallel and just beneath the free (111) surface at a depth of one atomic level [30].

When connected together, two pairs of partial dislocations (*i.e.* of different variants) form the well-known chevron-like pattern. For instance, the chevron pattern shown in Fig. 1 is related to the connection of the CA = Cδ + δA variant with the CB = Cδ + δB variant. Note that the Au(111)

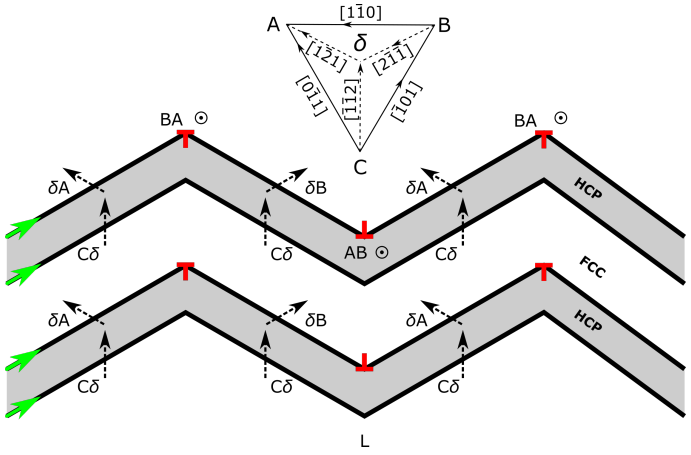

Figure 1: Schematic of the Au(111) surface reconstruction. Bold black lines represent partial dislocation lines. The green and the dotted arrows indicate the line direction and the Burgers vector of the partial Xδ (or δX) dislocations, respectively, in agreement with the Thompson tetrahedron. The threading dislocations AB and BA are symbolized with the red $\perp$ and have a unit line lying along the [111] direction perpendicularly to the free surface.

intersection of two partial dislocations can lead to a perfect edge dislocation AB (or BA) lying perpendicular to the free surface (see the red symbols $\perp$ in Fig. 1). Contrary to the partials, these dislocations emerge at the free surface [30] and are henceforth referred to as threading dislocations. Note that there are only two threading dislocations per unit chevron (see Fig. 1), so that the dislocation network is not invariant by rotation at 180°. It is noticed that such a dislocation network was already used to describe {111} surface reconstructions of other fcc materials [30, 31], as well as network of epitaxial dislocations [32, 33, 34, 12]. From a theoretical perspective, a dislocation can only move in the plane defined by its line and its Burgers vector. As all the partial dislocations can thus only move in the same plane (the one

parallel and just beneath the free surface), it is believed that the Au(111) reconstruction may be stress-driven by the threading dislocations AB and BA.

Gold single crystals, with a cross-section of $2\times2\,\mathrm{mm}^2$ and 6 mm in length, were first prepared in an ultra high vacuum (UHV) environment ($< 10^{-10}$ mbar) by sequences of Ar-sputtering (0.9 kV) and subsequent annealing at approximately 850 K for 15 min. The samples were then mechanically strained using a home-made experimental apparatus that allows investigation, *in situ* by UHV STM, of the evolution of sample surfaces under increasing strain. Microscopy can be carried out with this setup at variable temperature from 90 to 600 K and with uniaxial compression at strain rates between 10^{-6} to $10^{-2}\,\mathrm{s}^{-1}$ applied to the sample via two piezoelectric actuators. A more detailed description of the apparatus is provided elsewhere [29]. In this study, the gold single crystals were deformed at 300 K by uniaxial compression along the $[\bar{1}10]$ direction, with a strain rate of $7.10^{-6}\,\mathrm{s}^{-1}$.

A characteristic STM image of the Au(111) reconstruction after a few preparation cycles is shown in Fig. 2(a). V_1 and V_2 correspond to two unit vicinal steps. The hcp and fcc regions are clearly distinguishable due to the out-of-plane displacements of 20 ± 5 pm induced by the partial dislocation lines (white contrasts in Fig. 2), in good agreement with the literature [6]. It was shown that the BA (resp. AB) threading dislocations is locally associated with a significant enlargement (resp. narrowing) of the hcp area [20]. In addition, the fcc region width is larger than the hcp one [6]. These features allow unambiguous positioning of the characteristic threading AB and BA dislocations on the Au(111) reconstruction. See the symbols $\perp$ in Fig. 2(c)

which is an enlargement of Fig. 2(a) (defined by the dotted frame). AB and BA dislocations are aligned in walls and are labelled by a letter u, v or w depending on which wall they belong to and by a number 1, 2, 3 or 4 in reference to their corresponding chevron. For example, chevron 3, highlighted by a grey line in Fig. 2(c), is composed of u_3, v_3 and w_3 threading dislocations. The length of a unit chevron along the $[\bar{1}10]$ direction, *i.e.* between the two walls u and w, is found to be $L \approx 29\,\text{nm}$ and wall v is at equal distance from walls u and w in the unstressed state.

The same area is shown in Fig. 2(b) after a plastic strain of $\epsilon = 0.25\,\%$ (associated to an external stress $\sigma = 6\,\text{MPa}$). The single crystal has been sheared by a dislocation, leading at surface to the formation of a single slip trace T lying at approximately 60° from the compression axis, as expected from the crystal orientation. A re-organization of the reconstruction is observed close to the slip trace. It is characterized by U-shape patterns on the lower part of the step and results from the localized stress field induced by the step [27]. Molecular dynamics simulations have demonstrated that this stress vanishes beyond approximately 15 nm from the step [26]. Thus, it can be assumed that both the vicinal steps and the slip trace have not affected the chevron-like pattern in the region of Fig. 2 highlighted by the dotted frame. The enlargement of Fig. 2(b) is presented in Fig. 2(d) for $\epsilon = 0.25\,\%$. It is shown that the dislocation walls have been shifted in relation to each other. The distance L between u and w dislocation walls stays approximately constant, but the unit chevron is now asymmetrical, with the distance between u and v dislocation walls being now more than twice the distance between v and w. A close inspection reveals also that the distance in

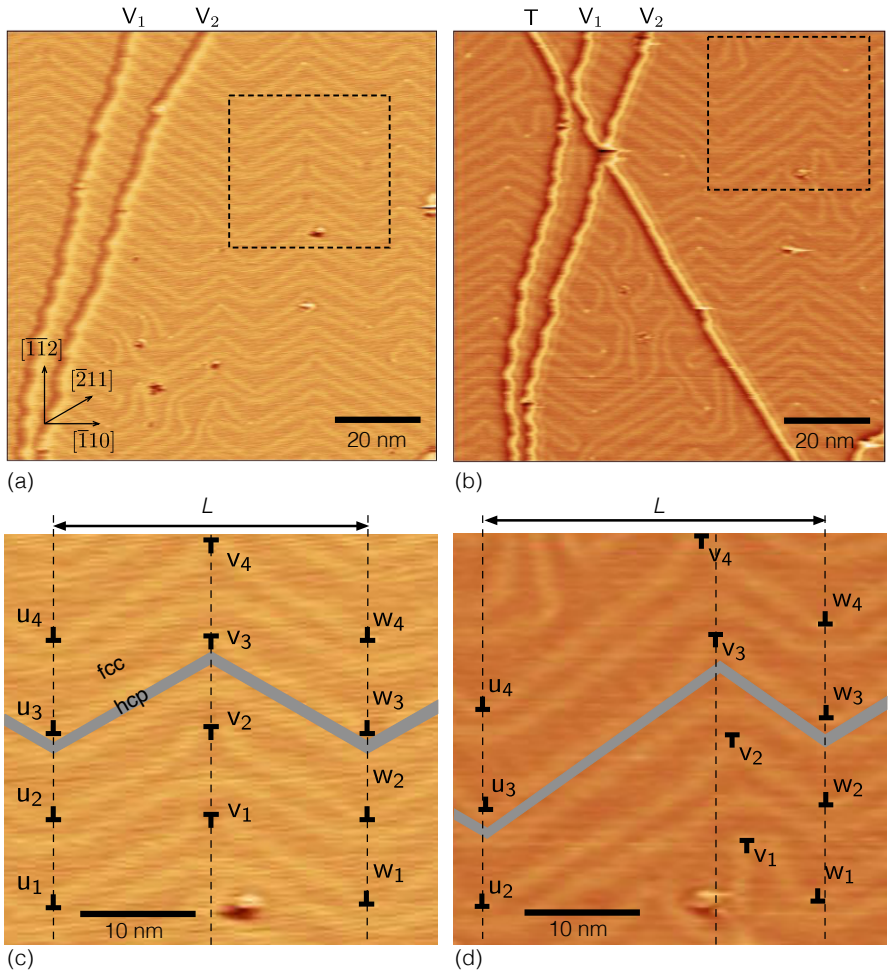

Figure 2: STM images of the Au(111) surface (a) before and (b) after plastic strain at room temperature by uniaxial compression along the $[\bar{1}10]$ direction ($\epsilon = 0.25\,\%$, $\sigma = 6\,\mathrm{MPa}$). An enlargement defined by the dotted grey frame in (a) and (b) is shown in (c) and (d), respectively. V_1 and V_2 correspond to vicinal steps, T to a single slip trace induced by the plastic increment. In (c) and (d), the AB and BA threading dislocations are labelled by black $\perp$ and by a symbol x_i, with $\mathsf{x} = \mathsf{u}, \mathsf{v}$ or w and i =1, 2, 3 or 4 referring to the wall and the chevron that the dislocations belong to, respectively. L is the length of a unit chevron. The grey line highlights the chevron 3.

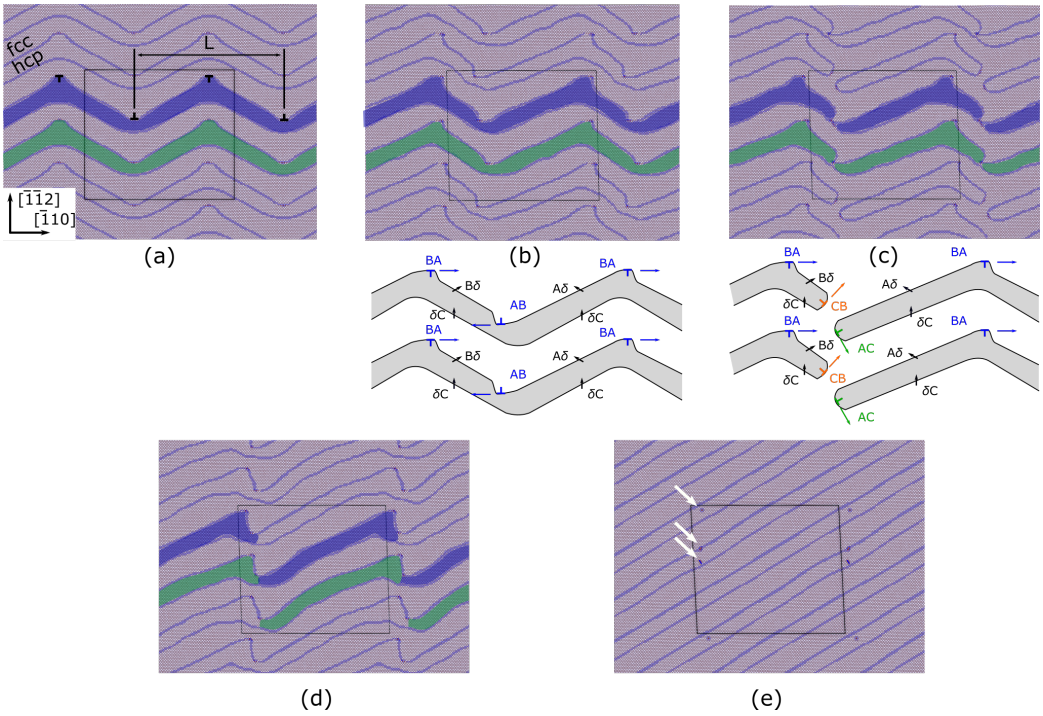

Figure 3: Evolution by molecular dynamics simulations at 300 K of the chevron pattern as a function of increasing tensile stress oriented at $-45°$ from the $[\bar{1}10]$ direction. For (a) no external stress, (b) $\sigma = 3.4\,\mathrm{GPa}$, (c) $\sigma = 4.0\,\mathrm{GPa}$, (d) $\sigma = 4.5\,\mathrm{GPa}$, (e) $\sigma = 5.7\,\mathrm{GPa}$. White arrows in (e) indicate the presence of adatoms or vacancies at the free surface. The black square represents the simulation box. Atoms are colored according to the number of first-neighboring atoms: light blue is for the atoms at free (111) surfaces and dark blue is for the atoms belonging to the partial dislocation lines that separate the hcp to the fcc areas. The dislocations shown in the schematics are referred to the Thompson tetrahedron (Fig. 1).

the $[\bar{1}\bar{1}2]$ direction has increased between u_i and v_i threading dislocations by approximately 6.5 nm and has decreased between v_i and w_i dislocations by less than 1.2 nm. The distances between threading dislocations in every wall u, v or w stay constant, meaning that the new chevron organization seems to have taken place everywhere in the region of interest. Note also that the chevron-like pattern may experimentally exhibit some surface defects or imperfections that could locally influence the dislocation organization. In Fig. 2(d) the new organization might be initiated in the lower part of the image, but the defect locally disturbs the dislocation line so that it appears curved around the defect instead of straight.

From a theoretical perspective, the re-organization of the chevron-like pattern can be explained by the collective displacement of the BA/AB threading dislocations under stress. A perfect edge dislocation (like AB and BA) can move in a direction either parallel (gliding mechanism) or perpendicular (climbing mechanism) to its Burgers vector [35]. Taking into account the orientation of the loading axis with respect to the Burgers vectors of AB and BA dislocations, the Schmid factor is equal to zero according to the elastic theory of dislocations [35]. As a consequence, no gliding force is expected to act on the dislocation line. A misorientation of the mechanical external compression axis with respect to the crystallographic $[\bar{1}10]$ direction may consequently explain the significant gliding of the threading dislocations observed in Fig. 2(b). Dislocation climb requires atomic diffusion, is therefore temperature dependent [35] and is usually considered as a mechanism less easily activated than dislocation glide. Although there is no evidence of atomic diffusion at the surface of the Au single crystal, climb could be

involved in the displacement of the threading dislocations and might explain their new positions in Fig. 2(d).

Molecular dynamics simulations using the LAMMPS code [36] have been carried out to study the influence of an external stress on the Au(111) reconstruction and describe how the displacement of BA/AB threading dislocations can drive the evolution of the herringbone pattern. Interactions between Au atoms are described by the second-nearest-neighbor modified embedded atom method (2nn-MEAM) potential parameterized by Lee *et al.* [37] and improved by Ryu *et al.* [38]. Three parameters describing the MEAM potential were adjusted to describe the $22 \times \sqrt{3}$ reconstruction of Au(111). All the modifications of the interatomic potential are described in a previous work [26]. Visualization of the atomic configurations is made using the Open Visualization Tool (OVITO) [39].

The method of building the chevron pattern is given in the Supplementary Material. Once the atomic configuration has been relaxed by a conjugate gradient algorithm, it is thermalized at 300 K for 300 ps, with a pressure maintained at a value of 0 GPa on the simulation box, by molecular dynamics simulations using the Nosé-Hoover thermo-barostat (NPT thermodynamic ensemble) and a time step of 1 fs. Periodic boundary conditions along $[\bar{1}10]$ and $[\bar{1}\bar{1}2]$ directions and free surfaces with normal direction [111] are considered. The initial structure (*i.e.* with no external stress) is shown in Fig. 3(a). As described previously, the BA (resp. AB) dislocations are located where the hcp area is enlarged (resp. narrowed) [20]. The length of the chevron is equal to L= 25.5 nm, in agreement with values typically observed through STM.

The atomic configuration is mechanically loaded by applying to the simulation box an uniaxial tensile stress σ at $-45°$ from the $[\bar{1}10]$ direction, leading to a maximum glide force $\sigma b/2$ on AB/BA dislocations, with b the magnitude of the Burgers vector. The climb force is not zero and takes an intermediate value also equal to $\sigma b/2$. But, in tension, dislocation climb implies exchange of atoms from adatoms covering the surface into the surface layer, and, in our simulation, it should hardly be activated owing to the absence of any reservoir of atoms. Therefore, the loading condition considered in the simulation aims at investigating how the herringbone pattern is modified by the only glide of threading dislocations. To implement the desired loading conditions, the configuration is elongated in the tension direction by a strain $\varepsilon > 0$ and contracted in the perpendicular direction by a strain $-\nu\varepsilon$, with $\nu = 0.547$ the Poisson ratio computed from the elastic coefficients values $C_{11} = 203.5\,\text{GPa}$, $C_{12} = 169.3\,\text{GPa}$ and $C_{44} = 42.5\,\text{GPa}$ in the perpendicular direction. The uniaxial stress is given by $\sigma = E\varepsilon$, with $E = 88\,\text{GPa}$. A molecular dynamics simulation is then performed at a strain rate $\dot{\varepsilon} = 3.10^8\,\text{s}^{-1}$ and at 300 K using a Nosé-Hoover thermostat (NVT thermodynamic ensemble).

The evolution of the chevron-like pattern is presented in Fig. 3(b)-(e) for increasing mechanical stress at 300 K. The BA and AB dislocations first glide along opposite directions, due to their opposite Burgers vectors (Fig. 3(b) at $\sigma = 3.4\,\text{GPa}$). The AB dislocation moves consequently towards the δC partial dislocation, constricting the hcp region. For convenience, schematics have been added to highlight the dislocation mechanisms. At $\sigma = 4.0\,\text{GPa}$, once AB dislocations have intersected δC dislocations, they dissociate into two AC and CB threading dislocations which connect Aδ and Bδ partial dislocations

to δC ones, respectively. Such a mechanism allows the hcp regions to locally disappear producing two hcp arms that are free to move according to the degrees of freedom of AC and CB dislocations located at their extremities (Fig. 3(c)). These two newly created threading dislocations have a non zero Schmid factor. They glide along their slip direction and a CB dislocation of one chevron recombines with the AC dislocation of the upper one (Fig. 3(d)) to restore AB dislocations. These elementary plastic mechanisms lead to the shearing of the chevron configuration and contribute to the lengthening of one arm of the chevrons with respect to the other. Additionally, it shows that the chevron pattern evolution results only from the glide of threading dislocations and that dislocation climb is not required to be activated. Finally, increasing the stress up to $\sigma = 5.7\,\mathrm{GPa}$ (Fig. 3(e)) allows a second shearing of the chevrons to occur, similar to the first in terms of dislocation glide, dissociations and recombinations. AB dislocations resulting from this second step annihilate with BA dislocations. The final pattern is thus composed of straight partial dislocations lying along the $[\bar{2}11]$ direction, with no more threading dislocations AB or BA at the free Au(111) surface. As AB and BA are not exactly gliding in the same plane along the $[\bar{1}10]$ direction, their annihilation results from climbing and produces adatoms and vacancies at the surface of the crystal (see the white arrows in Fig. 3(e)).

Scanning tunneling microscopy investigations have highlighted that an external applied stress can modify the Au(111) reconstruction by moving the threading dislocations. Molecular dynamics simulation has confirmed that the threading dislocations are mobile under stress, driving the subsurface partial dislocation network. It has been shown that the chevron-like pattern

can be modified to an assymetrical configuration, only by considering glide, dissociation and recombination of the threading dislocations, without the need for their climb. The stress at which this evolution occurs is found to be several decades higher in the simulation than in experiment, because of the very high value of the strain rate that is usually required in molecular dynamics simulations. The annihilation of all the threading dislocations is numerically found at high stresses leading to a periodic pattern of hcp stripes aligned along the $[\bar{1}\bar{1}2]$ direction, but has not been experimentally observed on our gold single crystals. It may be explained by too many defects at the free surface, such as imperfections, contaminations, vicinal steps or slip traces, that may locally disturb the expected pattern or by plastic relaxation of the Au single crystal that prevents the applied stress to be high enough. It should be said, however, that similar periodic pattern over a large area has already been obtained in the past on strained mica wafers coated by gold thick films on which the density of defects looks very small [28]. It is believed that the presently reported phenomenon gives new insight into how an atomic reconstruction can be modulated and controlled by nanomechanical engineering, in order to be further used as a template for conferring new functional properties to materials.

Supplementary Material

See the supplementary material in which a description of the method of building the chevron pattern is given.

Acknowledgments

This work was partially funded by the French Government program "Investissements d'Avenir" (LABEX INTERACTIFS, reference ANR-11-LABX-0017-01). Computations have been performed on the supercomputer facilities of the 'Mésocentre de calcul Poitou-Charentes'.

References

[1] M. Poensgen, J. F. Wolf, J. Frohn, M. Giesen, H. Ibach, Step dynamics on Ag(111) and Cu(100) surfaces, Surf. Sci. 274 (1992) 430–440. doi:10.1016/0039-6028(92)90848-Z.

[2] S. Yoshida, T. Sekiguchi, K. M. Itoh, Atomically straight steps on vicinal Si(111) surfaces prepared by step-parallel current in the kink-up direction, Appl. Phys. Lett. 87 (2005) 031903. doi:10.1063/1.1995946.

[3] P. Campiglio, V. Repain, C. Chacon, O. Fruchart, J. Lagoute, Y. Girard, S. Rousset, Quasi unidimensional growth of Co nanostructures on a strained Au(111) surface, Surf. Sci. 605 (2011) 1165–1169. doi:10.1016/j.susc.2011.03.019.

[4] Y. Tabuchi, K. Ashida, M. Sonoda, T. Kaneko, N. Ohtani, M. Katsuno, S. Sato, H. Tsuge, T. Fujimoto, Wide (0001) terrace formation due to step bunching on a vicinal 4H-SiC (0001) epitaxial layer surface, J. Appl. Phys. 122 (2017) 075702. doi:10.1063/1.4999480.

[5] S. Bin Anooz, R. Grüneberg, C. Wouters, R. Schewski, M. Albrecht, A. Fiedler, K. Irmscher, Z. Galazka, W. Miller, G. Wagner,

J. Schwarzkopf, A. Popp, Step flow growth of β-Ga_2O_3 thin films on vicinal (100) β-Ga_2O_3 substrates grown by MOVPE, Appl. Phys. Lett. 116 (2020) 182106. doi:10.1063/5.0005403.

[6] J. V. Barth, H. Brune, G. Ertl, R. J. Behm, Scanning tunneling microscopy observations on the reconstructed Au(111) surface: Atomic structure, long-range superstructure, rotational domains, and surface defects, Phys. Rev. B 42 (1990) 9307. doi:10.1103/PhysRevB.42.9307.

[7] V. Repain, J. M. Berroir, S. Rousset, J. Lecoeur, Interaction between steps and reconstruction, App. Surf. Sci. 162 (2000) 30–41. doi:10.1016/S0169-4332(00)00166-5.

[8] S. Rohart, G. Baudot, V. Repain, Y. Girard, S. Rousset, H. Bulou, C. Goyhenex, L. Proville, Atomistic mechanisms for the ordered growth of Co nanodots on Au(788): a comparison between VT-STM experiments and multi-scaled calculations, Surf. Sci. 559 (2004) 47–62. doi:10.1016/j.susc.2004.03.064.

[9] M. Jäger, A. Teker, J. Mannhart, W. Braun, Independence of surface morphology and reconstruction during the thermal preparation of perovskite oxide surfaces, Appl. Phys. Lett. 112 (2018) 111601. doi:10.1063/1.5023318.

[10] M. Hu, Q. Zhang, L. Gu, Q. Guo, Y. Cao, M. Kareev, J. Chakhalian, J. Guo, Reconstruction-stabilized epitaxy of $LaCoO_3/SrTiO_3$(111) heterostructures by pulsed laser deposition, Appl. Phys. Lett. 112 (2018) 031603. doi:10.1063/1.5006298.

[11] S. Curiotto, F. Cheynis, F. Leroy, P. Müller, Surface diffusion of Au on 3×3 Si(111)–Au studied by nucleation-rate and Ostwald-ripening analysis, Surf. Sci. 647 (2016) 8–11. doi:10.1016/j.susc.2015.11.015.

[12] A. Fleurence, Y. Yamada-Takamura, Adatom-induced dislocation annihilation in epitaxial silicene, arXiv:2010.07519 (2020).

[13] C. Wöll, S. Chiang, R. J. Wilson, P. H. Lippel, Determination of atom positions at stacking-fault dislocations on Au(111) by scanning tunneling microscopy, Phys. Rev. B. 39 (1989) 7988. doi:10.1103/PhysRevB.39.7988.

[14] K. G. Huang, D. Gibbs, D. M. Zehner, A. R. Sandy, S. G. J. Mochrie, Phase behavior of the Au(111) surface: Discommensurations and kinks, Phys. Rev. Lett. 65 (1990) 3313. doi:10.1103/PhysRevLett.65.3313.

[15] M. Böhringer, K. Morgenstern, W.-D. Schneider, R. Berndt, F. Mauri, A. De Vita, R. Car, Two-dimensional self-assembly of supramolecular clusters and chains, Phys. Rev. Lett. 83 (1999) 324–327. doi:10.1103/PhysRevLett.83.324, publisher: American Physical Society.

[16] O. Ourdjini, R. Pawlak, S. Clair, L. Chen, N. Bergeon, M. Sassi, V. Oison, J. Debienrre, R. Coratger, L. Porte, Substrate-mediated ordering and defect analysis of a surface covalent organic framework, Phys. Rev. B 84 (2011) 125421. doi:10.1103/PhysRevB.84.125421.

[17] T. Jasper-Tönnies, M. Gruber, S. Karan, H. Jacob, F. Tuczek, R. Berndt, Deposition of a cationic FeIII spin-crossover complex on

Au(111): Impact of the counter Io, J. Phys. Chem. Lett. 559 (2017) 1569–1573. doi:10.1021/acs.jpclett.7b00457.

[18] C. Casari, S. Foglio, F. Siviero, A. Li Bassi, M. Passoni, C. Bottani, Direct observation of the basic mechanisms of Pd island nucleation on Au(111), Phys. Rev. B 79 (2009) 195402. doi:10.1103/PhysRevB.79.195402.

[19] O. Fruchart, M. Klaua, B. J, J. Kirschner, Self-Organized Growth of Nanosized Vertical Magnetic Co Pillars on Au(111), Phys. Rev. Lett. 83 (1999) 2769. doi:10.1103/PhysRevLett.83.2769.

[20] M. Corso, L. Fernández, F. Schiller, J. E. Ortega, Au(111)-based nanotemplates by Gd alloying, ACS Nano 4 (2010) 1603–1611. doi:10.1021/nn901345s.

[21] M. M. Biener, J. Biener, R. Schalek, C. M. Friend, Surface alloying of immiscible metals: Mo on Au(111) studied by STM, Surf. Sci. 594 (2005) 221–230. doi:10.1016/j.susc.2005.07.028.

[22] J. V. Barth, G. Constantini, K. Kern, Energies of the atomic steps formed on low index surfaces of fcc metals, Nature 437 (2005) 671–679. doi:10.1038/nature04166.

[23] R. Pawlak, J. G. Vilhena, A. Hinaut, T. Meier, T. Glatzel, A. Baratoff, E. Gnecco, R. Pérez, E. Meyer, Conformations and cryo-force spectroscopy of spray-deposited single-strand DNA on gold, Nat. Commun. 10 (2019) 1–7. doi:10.1038/s41467-019-08531-4.

[24] V. Repain, J. M. Berroir, S. Rousset, J. Lecoeur, Interaction between steps and reconstruction on Au(111), Europhys. Lett. 47 (1999) 435. doi:10.1209/epl/i1999-00406-6.

[25] S. Rousset, V. Repain, G. Baudot, Y. Garreau, J. Lecoeur, Self-ordering of Au(111) vicinal surfaces and application to nanostructure organized growth, J. Phys.: Condens. Matter. 15 (2003) S3363–S3392. doi:10.1088/0953-8984/15/47/009, publisher: IOP Publishing.

[26] D. Chauraud, J. Durinck, M. Drouet, L. Vernisse, J. Bonneville, C. Coupeau, Influence of terrace widths on Au(111) reconstruction, Phys. Rev. B 96 (2017) 045410. doi:10.1103/PhysRevB.96.045410.

[27] D. Chauraud, J. Durinck, M. Drouet, L. Vernisse, J. Bonneville, C. Coupeau, How slip traces modify the Au(111) reconstruction, Phys. Rev. B 99 (2019) 195404. doi:10.1103/PhysRevB.99.195404.

[28] O. Schaff, A. Schmid, N. Bartelt, J. de la Figuera, R. Hwang, In-situ STM studies of strain-stabilized thin-film dislocation networks under applied stress, Mat. Sci. Eng. A-Struct 319 (2001) 914–918. doi:10.1016/S0921-5093(01)00977-7.

[29] Y. Nahas, F. Berneau, J. Bonneville, C. Coupeau, M. Drouet, B. Lamongie, M. Marteau, J. Michel, P. Tanguy, C. Tromas, An experimental UHV AFM-STM device for characterizing surface nanostructures under stress/strain at variable temperature, Rev. Sci. Instrum. 84 (2013) 105117. doi:10.1063/1.4826555.

[30] C. Carter, R. Hwang, Dislocations and the reconstruction of (111) fcc metal surfaces, Phys Rev. B 51 (1995) 4730–4733. doi:10.1103/PhysRevB.51.4730.

[31] A. Schmid, N. Bartelt, H. J.C, C. Carter, R. Hwang, Brownian motion of dislocations in thin films, Phys. Rev. Lett. 78 (1997) 3507–3510. doi:10.1103/PhysRevLett.78.3507.

[32] A. Fleurence, R. Friedlein, T. Ozaki, H. Kawai, Y. Wang, Y. Yamada-Takamura, Experimental evidence for epitaxial silicene on diboride thin films, Phys. Rev. Lett. 108 (2012) 245501. doi:10.1103/PhysRevLett.108.245501, publisher: American Physical Society.

[33] A. Fleurence, Y. Yamada-Takamura, Insights into the spontaneous formation of silicene sheet on diboride thin films, Appl. Phys. Lett. 110 (2017) 041601. doi:10.1063/1.4974467.

[34] J. d. l. Figuera, K. F. McCarty, N. C. Bartelt, Metastable misfit dislocations during thin-film growth: the case of Cu on Ru(0001), Surf. Sci. 682 (2019) 43–50. doi:10.1016/j.susc.2018.12.007.

[35] J. P. Hirth, J. Lothe, Theory of Dislocations, Wiley, New York, 1982.

[36] S. Plimpton, Computational limits of classical molecular dynamics simulations, Comp. Mater. Sci. 4 (1995) 361–364. doi:10.1016/0927-0256(95)00037-1.

[37] B.-J. Lee, J.-H. Shim, M. Baskes, Semiempirical atomic potentials for the fcc metals Cu, Ag, Au, Ni, Pd, Pt, Al, and Pb based on first and

second nearest-neighbor modified embedded atom method, Phys. Rev. B 68 (2003) 144112. doi:10.1103/PhysRevB.68.144112.

[38] S. Ryu, C. R. Weinberger, M. I. Baskes, W. Cai, Improved modified embedded-atom method potentials for gold and silicon, Model. Simul. Mater. Sc. 17 (2009) 075008–075008. doi:10.1088/0965-0393/17/7/075008.

[39] A. Stukowski, Visualization and analysis of atomistic simulation data with OVITO the open visualization tool, Model. Simul. Mater. Sci. Eng. 015012 (2010). doi:10.1088/0965-0393/18/1/015012.